

Characteristic Point Sequences in Local and Global Bifurcation Analysis of Filippov Systems

Ivan Arango
Universidad EAFIT
Department of Mechanics Engineering
Kra 42d 50 sur 40 Medellín
Colombia
iarango@eafit.edu.co

John Alexander Taborda
Universidad Nacional de Colombia
Department Electronics Engineering
Campus La Nubia Manizales
Colombia
yatabordag@unal.edu.co

Abstract: We explain the set of rules behind of the *LabView* toolbox for bifurcation analysis of Filippov systems denominated SPTCont 1.0. This software can detect nonsmooth bifurcations in n -dimensional systems using integration-free algorithms based on the evaluation of the vector fields on the discontinuity boundary (DB). In this paper, we present the characteristic point sequences that the software detects to guarantee the existence of local and global nonsmooth bifurcations in planar Filippov systems ($n = 2$). These sequences can be extended to three-dimensional or higher dimension Filippov systems. Boolean-valued functions are used to formulate the conditions of existence for each point defined in the sequences. Dynamics on DB and cycles are defined in function of the set of points. The full catalog of codim 1 local and global bifurcations is used to define the characteristic point sequence when the bifurcation parameter is varied. Finally, an illustrative example is analyzed using step-by-step routines of SPTCont 1.0.

Key-Words: Bifurcation theory, sliding bifurcations, piecewise-smooth systems, Filippov systems.

1 Introduction

Nonsmooth dynamics can be found in many physical systems such as electric motors, power converters, brakes, gears and joints. Switchings in electrical systems [1], [2], impacting motion in mechanical systems [3], [4], stick-slip motion in oscillators with friction [5], [6] and hybrid dynamics in control systems [7] are being studied with nonsmooth dynamical theory.

Nonsmooth characteristics were often neglected in mathematical models due to their difficulties of analysis and simulation. Actually, there is great interest to understand nonsmooth effects to try to minimise undesirable consequences such as wear of components, surface damage, fatigue failure and noise [8]. Many considerations based on bifurcations theory for smooth systems are violated and many new phenomena are observed such as sliding, crossing or grazing bifurcations.

Figure 1(a) shows a basic example of nonsmooth system. The undamped dry friction oscillator comprises a block resting on a belt, moving with velocity v . The motion of block with mass m along the belt is opposed by a spring (with stiffness k) connected to a fixed support. The spring exerts a restoring force on the block that is opposed by the friction force created by the belt. This system can be modelled with the

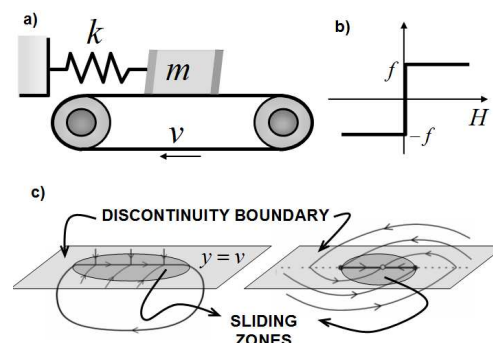


Figure 1: Basic example of nonsmooth systems: (a). Undamped dry friction oscillator on a rotating belt. (b). Coulomb friction model (H is the relative velocity). (c). Nonsmooth dynamics with sliding motion.

equation given in (1).

$$m\ddot{x} + kx = f \operatorname{sgn}(v - \dot{x}) \quad (1)$$

In an equivalent way, this system can be expressed with the non-dimensionless system of first order ODEs given by equation (2).

$$\begin{cases} \dot{x} = y \\ \dot{y} = -x + f \operatorname{sgn} H \quad \text{where} \quad H = (v - y) \end{cases} \quad (2)$$

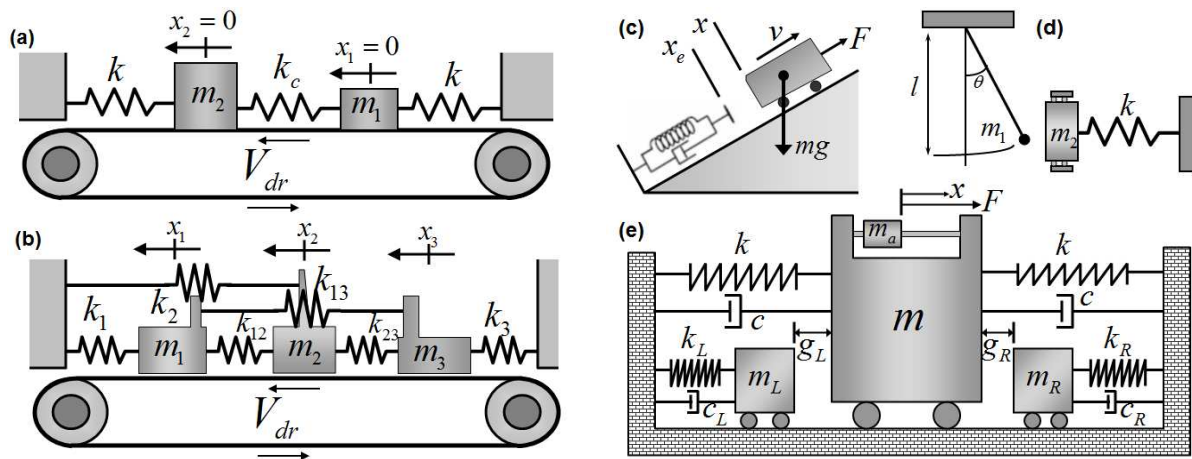


Figure 2: Examples more complex of nonsmooth systems. (a). Friction oscillator with two masses, (b). Friction oscillator with three masses, (c). Mechanical model with gravitational force, (d)., Pendulum-car model and (e). Friction oscillators with impact.

The Coulomb friction model is presented in figure 1(b) according to equation (3). When the velocity of the block is less than the velocity of the belt the friction is positive and constant and when the velocity of the block is greater than that of the belt the friction is negative.

$$F = \begin{cases} +f, & y < v \\ -f, & y > v \end{cases} \quad (3)$$

Systems where sliding motion is possible are known as Filippov systems. In the simple Filippov system presented in figure 1(a), the block will move with the belt until the spring tension increases enough to overcome the frictional force and then the block will start to move again. These zones are known as sliding zones due to the system forcing the motion to slide along the surface before it can leave to join another vector field. Examples of nonsmooth dynamics with sliding motion are presented in figure 1(c). When the sliding motion on the discontinuity boundary (DB) is possible, the analysis is more complicated. Moreover, the complexity can increase when the number of elements with nonsmooth interaction (as masses) is higher or when impacts motions are possible. Examples of Filippov systems with more complex models are presented in figure 2 [9], [7].

We explain the set of rules behind of the *LabView* toolbox for bifurcation analysis of Filippov systems denominated *SPTCont 1.0*. The paper is organized as follows. In section II we present the generalities of *SPTCont 1.0* while the concepts of Filippov systems and the SPT method are presented in section III. Dynamics on DB and cycles in function of the characteristic points are summarized in the section IV. In

the sections V and VI we present the characteristic point sequences for representative local and global bifurcations, respectively. An illustrative example is detailed in section VII. Finally, the conclusions and future work are discussed in the section VIII.

2 Generalities of SPTCont 1.0

The number of specialized software in nonsmooth dynamics is reduced [10], [11]. In [12] and [6], they are presented two toolboxes for analysis and continuation of nonsmooth bifurcations in Filippov systems. The platforms used in these toolboxes are Matlab and AUTO97.

A LabView toolbox was proposed in [13] for bifurcation analysis of Filippov systems denominated *SPTCont 1.0*. LabView platform allows the development of user interface with graphical controls and indicators easily. Also, the fully object-oriented character of LabVIEW code allows functions reuse without modifications.

SPTCont 1.0 toolbox is included in the *GAONDYSY* software developed with language G for analysis of non-smooth dynamical systems [14]. Many libraries of LabVIEW with functions of graphics generation, mathematics and data analysis are used too. *SPTCont 1.0* uses integration-free algorithms based on the evaluation of the vector fields on the discontinuity boundary (DB). The routines apply the classification of points and events on DB recently proposed [15], [16], [17]. Local and global bifurcations can be detected using the numerical method *Singular Point Tracking* or *SPT*.

This software can detect nonsmooth bifurcations

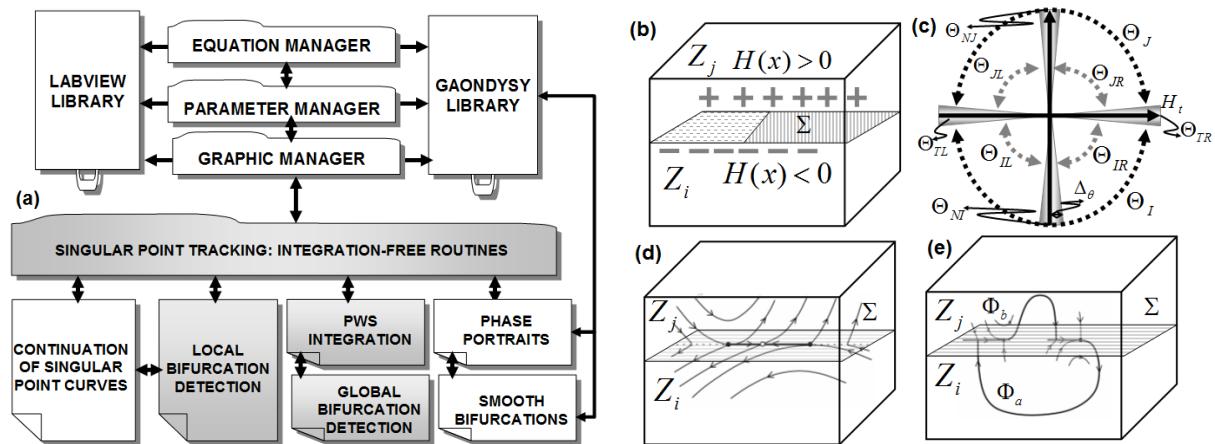


Figure 3: (a). SPTCont structure with integration-free algorithms, (b). Vector fields and discontinuity boundary (DB), (c). Angular ranges in the analysis point on DB, (d)., Example of local dynamic (e). Example of global dynamic.

in n -dimensional systems using integration-free algorithms based on the evaluation of the vector fields on the discontinuity boundary (DB).

In the figure 3(a) we present the general structure of the SPTCont 1.0. The input of the equations and the parameters are managed for different windows using the same environment of GAONDYSY [14]. In the same way, the outputs are data of graphics have independent windows. The graphical elements are provided by the LabVIEW package.

Depending on the Filippov system dimension (2D, 3D, ..., nD) is executed a different SPT (Singular Point Tracking) routine. In the case 2D, the discontinuity boundary (DB) is a line, while in the case 3D the DB is plane. Modules for continuation of non-smooth bifurcations, detection of local and global bifurcations and generation of phase portraits are integrated to the SPTCont 1.0 toolbox.

Two principal advantages have the software in the analysis of nonsmooth systems. First, the software has educational and didactic subroutines for amateur users. Second, the software has functions for specialized users where the integration-free algorithms in the SPT avoid the well known numerical problems of these algorithms. If the integration is unavoidable, for example in detection of global bifurcations, the SPT method computes the initial condition of the simulation to reduce the compute time. The SPTCont 1.0 was proven with the catalog of local and global bifurcations that it was proposed recently in [18].

In the next section, Filippov systems are defined and the SPT is explained. The set of rules behind of SPTCont 1.0 toolbox are given in function of the points defined using Boolean-valued functions $B(\cdot)$

that return True or False when their arguments are evaluated. In these functions we use the logical connectives AND, OR and NOT denoted by \wedge , \vee and \neg , respectively.

3 Filippov Systems and SPT method

Let $\{\mathbf{F}_i(\mathbf{x}), \mathbf{F}_j(\mathbf{x}), H(\mathbf{x})\}$ be a set of equations that defines the piecewise-smooth autonomous system (denominated Filippov system) given by equation (4) where $\mathbf{x} \in R^2$ and $\alpha \in R$ is the bifurcation parameter.

$$\begin{aligned} \dot{\mathbf{x}} &= \begin{cases} \mathbf{F}_i(\mathbf{x}, \alpha) & \text{if } \mathbf{x} \in Z_i \\ \mathbf{F}_j(\mathbf{x}, \alpha) & \text{if } \mathbf{x} \in Z_j \end{cases} \\ \Sigma &= \{\mathbf{x} \in R^2 : H(\mathbf{x}, \alpha) = 0\} \\ Z_i &= \{\mathbf{x} \in R^2 : H(\mathbf{x}, \alpha) < 0\} \\ Z_j &= \{\mathbf{x} \in R^2 : H(\mathbf{x}, \alpha) > 0\} \end{aligned} \quad (4)$$

Filippov systems can be described by a set of first-order ordinary differential equations with a discontinuous right-hand side [19]. The vector fields \mathbf{F}_i and \mathbf{F}_j are sufficiently smooth vector functions and Z_i and Z_j are Smooth Zones. The discontinuity boundary, (DB) denoted by Σ , is defined by the scalar function $H(\mathbf{x})$. The sign of $H(\mathbf{x})$ indicates a smooth zone that is bounded by the DB (figure 3(b)).

In the last years, the dynamical and bifurcation behavior of Filippov systems has been studied widely [20], [18], [21], [22], [23], [24]. In Filippov systems, the sliding motion is possible. A lot of papers have been restricted to systems without sliding motion because the analysis is more simplified [18].

An analysis point \mathbf{x}_b on the DB ($\mathbf{x}_b \in \Sigma$) is defined and the normal vector (\mathbf{H}_n) and tangent vector (\mathbf{H}_t) to the DB in \mathbf{x}_b are computed. In this point, the

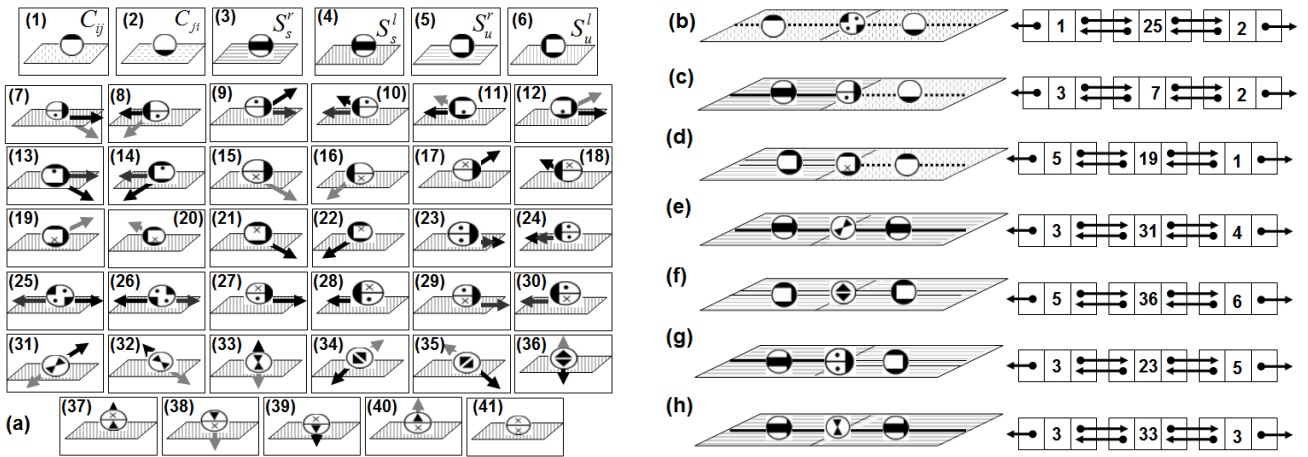


Figure 4: (a). Non-singular and singular points on DB. (b). to (h). Examples of typical combinations of points on DB.

vector fields \mathbf{F}_i and \mathbf{F}_j are evaluated. With reference to \mathbf{H}_t , the angles of vector fields φ_i and φ_j in anti-clockwise direction are computed. These angles are given by (5).

$$\varphi_{(i,j)} = \begin{cases} \theta_{(i,j)} & \text{if } F_{(i,j)y} \geq 0 \\ 2\pi - \theta_{(i,j)} & \text{if } F_{(i,j)y} < 0 \end{cases} \quad (5)$$

where $F_{(i,j)y}$ is the y-component of \mathbf{F}_i or \mathbf{F}_j and $\theta_{(i,j)}$ is given by:

$$\theta_{(i,j)} = \cos^{-1} \left(\frac{\langle \mathbf{H}_t, \mathbf{F}_{(i,j)} \rangle}{|\mathbf{H}_t| |\mathbf{F}_{(i,j)}|} \right) \quad (6)$$

The projections of each vector field in the vectors \mathbf{H}_t and \mathbf{H}_n are defined in this way: $F_i^n = \langle \mathbf{H}_n, \mathbf{F}_i \rangle$, $F_i^t = \langle \mathbf{H}_t, \mathbf{F}_i \rangle$, $F_j^n = \langle \mathbf{H}_n, \mathbf{F}_j \rangle$ and $F_j^t = \langle \mathbf{H}_t, \mathbf{F}_j \rangle$, where $\langle \dots, \dots \rangle$ denotes a scalar product.

Let $\Phi_a(\mathbf{x}, t)$ and $\Phi_b(\mathbf{x}, t)$ be the flows that take initial conditions \mathbf{x} in \mathbf{F}_i and \mathbf{F}_j , respectively (figure 3(e)).

$$\begin{cases} \frac{\partial}{\partial t} \Phi_a(\mathbf{x}, t) = \mathbf{F}_i(\Phi_a(\mathbf{x}, t)) & \Phi_a(\mathbf{x}, 0) = \mathbf{x} \\ \frac{\partial}{\partial t} \Phi_b(\mathbf{x}, t) = \mathbf{F}_j(\Phi_b(\mathbf{x}, t)) & \Phi_b(\mathbf{x}, 0) = \mathbf{x} \end{cases} \quad (7)$$

The solutions of (4) are uniquely defined forward and backward in time. However, the system (4) is not invertible because the orbits can overlap on DB with sliding [18](figure 3(d)). In sliding situations, a convex combination $\mathbf{G}(x)$ of the vectors \mathbf{F}_i and \mathbf{F}_j is defined as the *Filippov Method* [25]. The \mathbf{G} vector can be written as:

$$\mathbf{G}(\mathbf{x}) = \lambda \mathbf{F}_i(\mathbf{x}) + (1 - \lambda) \mathbf{F}_j(\mathbf{x}) \quad (8)$$

where,

$$\lambda = \frac{\langle \mathbf{H}_t(\mathbf{x}), \mathbf{F}_j(\mathbf{x}) \rangle}{\langle \mathbf{H}_t(\mathbf{x}), \mathbf{F}_j(\mathbf{x}) - \mathbf{F}_i(\mathbf{x}) \rangle} \quad (9)$$

The projection of $\mathbf{G}(\mathbf{x})$ in the vectors \mathbf{H}_t and \mathbf{H}_n are: $G^t = \langle \mathbf{H}_t, \mathbf{G} \rangle$ and $G^n = \langle \mathbf{H}_n, \mathbf{G} \rangle$. Using G^t are defined the Boolean-valued functions: \hat{M}_L and \hat{M}_R . The sliding motion is toward the right if \hat{M}_R is TRUE and the sliding motion is toward the left if \hat{M}_L is TRUE (equation (10)).

$$\begin{cases} M_R = B(G^t(x_b) > 0) \\ M_L = B(G^t(x_b) < 0) \end{cases} \quad (10)$$

Knowledge of the point types on DB is important to define *state portraits* of (4). Any *homeomorphism* $h : R^2 \rightarrow R^2$ should map the sliding and crossing segments of the original system onto the sliding and crossing segments of the transformed system, therefore, we can study generic systems and then apply *topological equivalence* criterions.

Ranges of angles are defined to evaluate the conditions of each vector fields and to characterize each point type. These ranges are referenced to \mathbf{H}_t and they are presented in the figure 3(c).

Two main ranges are considered: $\Theta_J = \{\theta \in (0, \pi)\}$ and $\Theta_I = \{\theta \in (\pi, 2\pi)\}$. A tolerance angle Δ_θ is defined (with $\Delta_\theta \rightarrow 0$) to detect the critical values: $\theta = 0$ and $\theta = \pi$.

The main ranges (Θ_J and Θ_I) and the auxiliary ranges ($\Theta_{JR}, \Theta_{JL}, \Theta_{IR}, \Theta_{IL}$) are defined in function of Δ_θ as they are presented in the equation 11. The tangent and normal angles are converted in ranges of

angles too, as they are presented in the equation (12).

$$\left\{ \begin{array}{l} \Theta_J = (\Delta\theta, \pi - \Delta\theta) \\ \Theta_I = (\pi + \Delta\theta, 2\pi - \Delta\theta) \\ \Theta_{JR} = (\Delta\theta, \pi/2 - \Delta\theta) \\ \Theta_{JL} = (\pi/2 + \Delta\theta, \pi - \Delta\theta) \\ \Theta_{IL} = (\pi + \Delta\theta, 3\pi/2 - \Delta\theta) \\ \Theta_{IR} = (3\pi/2 + \Delta\theta, 2\pi - \Delta\theta) \end{array} \right. \quad (11)$$

$$\left\{ \begin{array}{l} \Theta_{TR} = (2\pi - \Delta\theta, \Delta\theta) \\ \Theta_{TL} = (\pi - \Delta\theta, \pi + \Delta\theta) \\ \Theta_{NJ} = (\pi/2 - \Delta\theta, \pi/2 + \Delta\theta) \\ \Theta_{NI} = (3\pi/2 - \Delta\theta, 3\pi/2 + \Delta\theta) \end{array} \right. \quad (12)$$

Boolean-valued functions $B(\cdot)$ are defined using the angular ranges of the equations (11) and (12). Both angles φ_i and φ_j are computed and evaluated in the set of boolean rules. A typo of point on DB is defined depending on the boolean results.

The boolean-valued functions for the main ranges Θ_I and Θ_J are presented in the equation (13).

$$\left\{ \begin{array}{l} B_I^i = B(\varphi_i \in \Theta_I) \quad B_I^j = B(\varphi_j \in \Theta_I) \\ B_J^i = B(\varphi_i \in \Theta_J) \quad B_J^j = B(\varphi_j \in \Theta_J) \end{array} \right. \quad (13)$$

The boolean-valued functions for the auxiliary ranges Θ_{IR} , Θ_{IL} , Θ_{JR} and Θ_{JL} are presented in the equation (14).

$$\left\{ \begin{array}{l} B_{IR}^i = B(\varphi_i \in \Theta_{IR}) \quad B_{IR}^j = B(\varphi_j \in \Theta_{IR}) \\ B_{IL}^i = B(\varphi_i \in \Theta_{IL}) \quad B_{IL}^j = B(\varphi_j \in \Theta_{IL}) \\ B_{JR}^i = B(\varphi_i \in \Theta_{JR}) \quad B_{JR}^j = B(\varphi_j \in \Theta_{JR}) \\ B_{JL}^i = B(\varphi_i \in \Theta_{JL}) \quad B_{JL}^j = B(\varphi_j \in \Theta_{JL}) \end{array} \right. \quad (14)$$

Special points are detected when the angles φ_i and φ_j are located in the ranges Θ_T or Θ_N , or when these angles are not defined in the whole range Θ . In these cases, the boolean-valued functions are given by the equation (15).

$$\left\{ \begin{array}{l} B_T^i = B(\varphi_i \notin \Theta_T) \quad B_T^j = B(\varphi_j \notin \Theta_T) \\ B_N^i = B(\varphi_i \notin \Theta_N) \quad B_N^j = B(\varphi_j \notin \Theta_N) \\ B_X^i = B(\varphi_i \notin \Theta) \quad B_X^j = B(\varphi_j \notin \Theta) \end{array} \right. \quad (15)$$

The boolean-valued functions in the specific tangent ranges Θ_{TR} and Θ_{TL} are presented in the equation (16).

$$\left\{ \begin{array}{l} B_{TR}^i = B(\varphi_i \in \Theta_{TR}) \quad B_{TR}^j = B(\varphi_j \in \Theta_{TR}) \\ B_{TL}^i = B(\varphi_i \in \Theta_{TL}) \quad B_{TL}^j = B(\varphi_j \in \Theta_{TL}) \end{array} \right. \quad (16)$$

While the boolean-valued functions in the specific normal ranges Θ_{NI} and Θ_{NJ} are presented in the equation (17).

$$\left\{ \begin{array}{l} B_{NI}^i = B(\varphi_i \in \Theta_{NI}) \quad B_{NI}^j = B(\varphi_j \in \Theta_{NI}) \\ B_{NJ}^i = B(\varphi_i \in \Theta_{NJ}) \quad B_{NJ}^j = B(\varphi_j \in \Theta_{NJ}) \end{array} \right. \quad (17)$$

Three types of points can be distinguished on the discontinuity boundary (DB): Crossing points (C), Sliding points (S) and Singular sliding points (Ω). Forty-one different points are characterized on DB using the Boolean-valued functions presented in the equations (13) to (17).

Figure 4(a) presents the symbol and the associated number of each point. The singular sliding points (Ω) can be divided into six subsets: Tangent points (Ω_T), Vanished points (Ω_V), Tangent-Tangent points (Ω_{Π}), Tangent-Vanished points (Ω_{Ψ}), Quadrant or Pseudo-equilibrium points (Ω_Q) and Quadrant-Vanished points (Ω_{ϕ}). The general conditions for the singular sliding points are presented in the equation (18).

$$\left\{ \begin{array}{l} T = B_T^i \vee B_T^j \quad V = B_X^i \vee B_X^j \quad \Pi = B_T^i \wedge B_T^j \\ \Psi = (B_T^i \wedge B_X^j) \vee (B_X^i \wedge B_T^j) \\ Q = B((\pi - \Delta\theta) < |\varphi_i - \varphi_j| < (\pi + \Delta\theta)) \\ \Psi = (B_X^i \wedge B_X^j) \vee (B_X^i \wedge B_N^j) \vee (B_N^i \wedge B_X^j) \end{array} \right. \quad (18)$$

Crossing and sliding flows are the predominant behaviors on DB of the Filippov systems. Depending on the direction of the crossing orbits, two crossing (C) points can be defined: C_{ij} and C_{ji} . Four sliding (S) points are determined depending on the stability and the sliding motion direction.

The analysis point \mathbf{x}_b is a crossing point from Z_i to Z_j if the boolean-valued function C_{ij} presented in the equation (20) is TRUE. The angles φ_i and φ_i are contained in the range Θ_J . The analysis point \mathbf{x}_b is a crossing point from Z_j to Z_i if the boolean-valued function C_{ji} presented in the equation (20) is TRUE. The angles φ_i and φ_i are contained in the range Θ_I .

$$C = \left\{ \begin{array}{l} 1) \quad C_{ij} = B_J^i \wedge B_J^j \\ 2) \quad C_{ji} = B_I^i \wedge B_I^j \end{array} \right. \quad (19)$$

Let S be a boolean-valued function defined as $S : \mathbf{x}_b \rightarrow \{\text{TRUE}, \text{FALSE}\}$, which return TRUE for a point \mathbf{x}_b in Σ where the vectors \mathbf{F}_i and \mathbf{F}_j are not anti-collinear and they are have nontrivial normal components of the opposed sign, and FALSE otherwise.

If the angle φ_i is contained in the range Θ_J and φ_j is contained in the range Θ_I then the point \mathbf{x}_b is

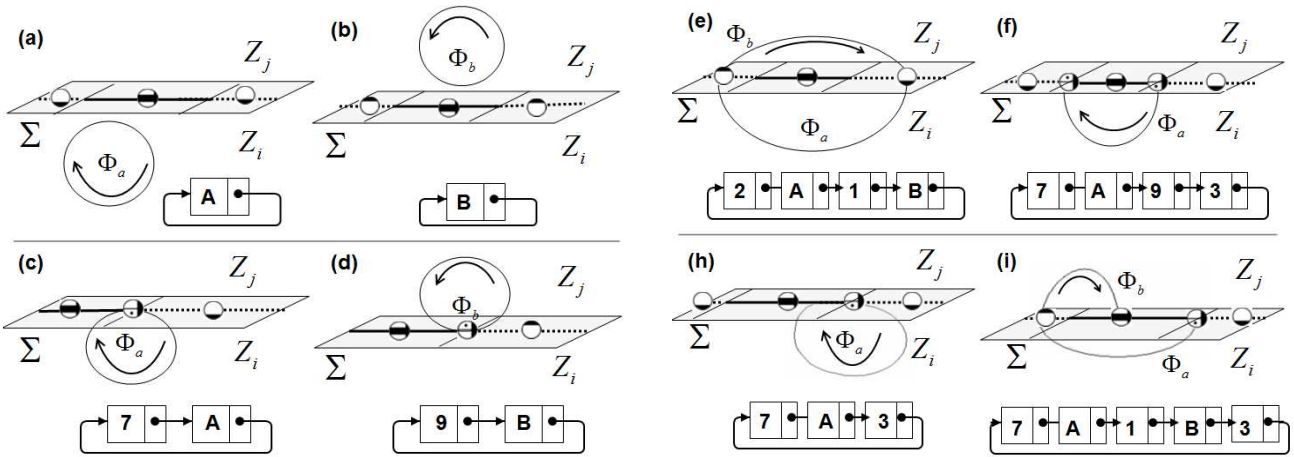


Figure 5: (a). and (b). Standard cycles L_{st} , (c). and (d). Grazing cycles, (e). Crossing cycle (f). Switching cycle, (g). and (h). Sliding cycles.

denominated *Stable sliding point* (S_s). If the angle φ_i is contained in the range Θ_I and φ_j is contained in the range Θ_J then the point \mathbf{x}_b is denominated *Unstable sliding point* (S_u). The sliding direction is defined with the equation (10).

$$S = \begin{cases} 3) & S_s^r = B_J^i \wedge B_I^j \wedge M_R \wedge \neg Q \\ 4) & S_s^l = B_J^i \wedge B_I^j \wedge M_L \wedge \neg Q \\ 5) & S_u^r = B_I^i \wedge B_J^j \wedge M_R \wedge \neg Q \\ 6) & S_u^l = B_I^i \wedge B_J^j \wedge M_L \wedge \neg Q \end{cases} \quad (20)$$

If \mathbf{x}_b belongs to Σ and C is FALSE and S is FALSE, then x_b is a singular sliding point. Six types of singular sliding point are defined:

- **Type Ω_T (Tangent):** The vector fields \mathbf{F}_i or \mathbf{F}_j are Tangents on the analysis point (\mathbf{x}_b).

Eight different points can be distinguished whose numerical codes and boolean-valued functions are given in equation (21). In each case \mathbf{F}_i or \mathbf{F}_j has null normal component.

$$\Omega_T = \begin{cases} 7) & T_i^{sr} = T \wedge B_I^j \wedge M_R \\ 8) & T_i^{sl} = T \wedge B_I^j \wedge M_L \\ 9) & T_j^{sr} = T \wedge B_J^i \wedge M_R \\ 10) & T_j^{sl} = T \wedge B_J^i \wedge M_L \\ 11) & T_i^{ur} = T \wedge B_J^j \wedge M_R \\ 12) & T_i^{ul} = T \wedge B_J^j \wedge M_L \\ 13) & T_j^{ur} = T \wedge B_I^i \wedge M_R \\ 14) & T_j^{ul} = T \wedge B_I^i \wedge M_L \end{cases} \quad (21)$$

- **Type Ω_T (Vanished):** The vector fields \mathbf{F}_i or \mathbf{F}_j are Vanished on the analysis point (\mathbf{x}_b).

Eight different points can be defined using the boolean-valued functions presented in equation (22). In these cases \mathbf{F}_i or \mathbf{F}_j have normal and tangent components equals to zero.

$$\Omega_V = \begin{cases} 15) & V_i^{sr} = V \wedge B_{IR}^j \wedge M_R \\ 16) & V_i^{sl} = V \wedge B_{IL}^j \wedge M_L \\ 17) & V_j^{sr} = V \wedge B_{JR}^i \wedge M_R \\ 18) & V_j^{sl} = V \wedge B_{JL}^i \wedge M_L \\ 19) & V_i^{ur} = V \wedge B_{JR}^j \wedge M_R \\ 20) & V_i^{ul} = V \wedge B_{JL}^j \wedge M_L \\ 21) & V_j^{ur} = V \wedge B_{IR}^i \wedge M_R \\ 22) & V_j^{ul} = V \wedge B_{IL}^i \wedge M_L \end{cases} \quad (22)$$

- **Type Ω_{II} (Tangent-Tangent):** The vector fields \mathbf{F}_i and \mathbf{F}_j are Tangents on the analysis point (\mathbf{x}_b).

Four different points are considered according to the boolean-valued functions presented in equation (23). Both vector fields \mathbf{F}_i and \mathbf{F}_j are tangents to DB.

$$\Omega_{II} = \begin{cases} 23) & \Pi_{rr} = B_{TR}^i \wedge B_{TR}^j \\ 24) & \Pi_{ll} = B_{TL}^i \wedge B_{TL}^j \\ 25) & \Pi_{rl} = B_{TR}^i \wedge B_{TL}^j \\ 26) & \Pi_{lr} = B_{TL}^i \wedge B_{TR}^j \end{cases} \quad (23)$$

- **Type Ω_{Ψ} (Tangent-Vanished):** The vector fields \mathbf{F}_i or \mathbf{F}_j are Tangents or they are vanished on the analysis point (\mathbf{x}_b).

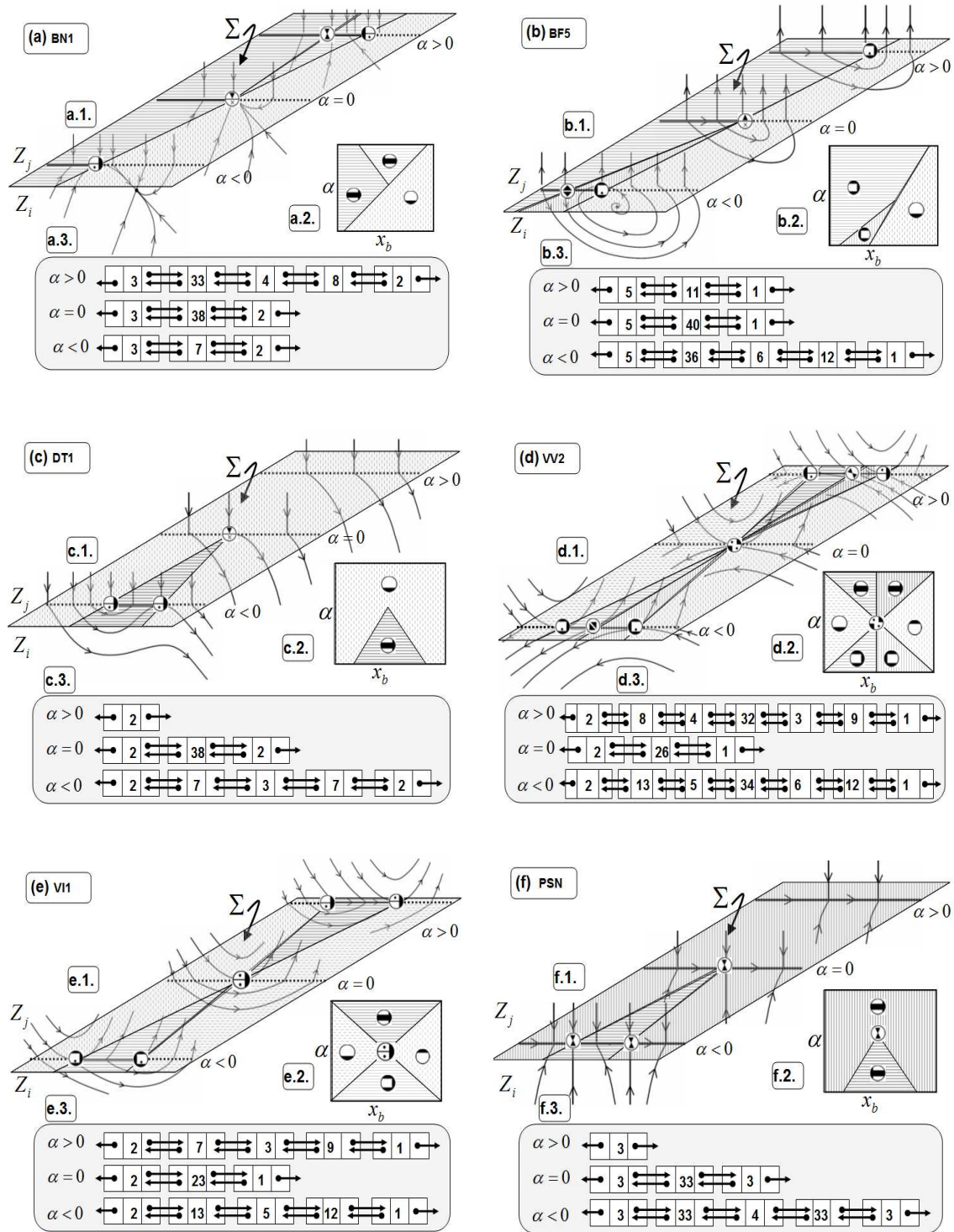


Figure 6: (1). Phase portraits of Local bifurcations. (2). DB bifurcation diagram. (3). Singular point sequences. (a) Boundary Node bifurcation (BN1) (b). Boundary Focus bifurcation (BF5). (c) Double Tangency bifurcation (DT1) (d). Two Tangencies Visible (VV2). (e) Visible-Invisible Tangencies bifurcation (VI1) (f). Pseudo-saddle-node bifurcation (PSN).

Four different points are defined and their boolean-valued functions are presented in equation (24). One vector fields is vanished and the other is tangent.

$$\Omega_{\Psi} = \begin{cases} 27) & \Psi_r^x = \Psi \wedge B_{TR}^i \\ 28) & \Psi_l^x = \Psi \wedge B_{TL}^i \\ 29) & \Psi_r^j = \Psi \wedge B_{TR}^j \\ 30) & \Psi_l^j = \Psi \wedge B_{TL}^j \end{cases} \quad (24)$$

– **Type Ω_Q (Quadrant):** The vector fields F_i and F_j are anti-collinear on the analysis point (\mathbf{x}_b).

Six different points are considered depending on the angular range where the condition Q (equation (18)) is satisfied. The numerical codes and the boolean-valued functions of the points Q are presented in equation (25).

$$\Omega_Q = \begin{cases} 31) & Q_{jr}^{il} = Q \wedge B_{JR}^i \\ 32) & Q_{jl}^{ir} = Q \wedge B_{JL}^i \\ 33) & Q_{nj}^{ni} = Q \wedge B_{NJ}^j \\ 34) & Q_{jr}^{jr} = Q \wedge B_{IL}^i \\ 35) & Q_{ir}^{jl} = Q \wedge B_{IR}^i \\ 36) & Q_{ni}^{nj} = Q \wedge B_{NI}^j \end{cases} \quad (25)$$

– **Type Ω_{ϕ} (Quadrant-Vanished):** The vector fields F_i or F_j are vanished and the other field is normal to H_t on the analysis point (\mathbf{x}_b).

Five different points are characterized with the boolean-valued functions given in equation (26).

$$\Omega_{\phi} = \begin{cases} 37) & \phi_{nj}^x = B_{NJ}^i \wedge B_X^j \\ 38) & \phi_x^{ni} = B_X^i \wedge B_{NI}^j \\ 39) & \phi_{ni}^x = B_{NI}^i \wedge B_X^j \\ 40) & \phi_x^{nj} = B_X^i \wedge B_{NJ}^j \\ 41) & \phi_x^x = B_X^i \wedge B_X^j \end{cases} \quad (26)$$

Each point has associated a symbol just as it is presented in the figure 4(a).

4 Modelling of Dynamics on DB and Sliding Cycles

In this section, we use the forty-one points defined in the previous section to analyze different scenarios on DB. Seven basic scenarios are determined. Figure 4 presents examples for each scenario.

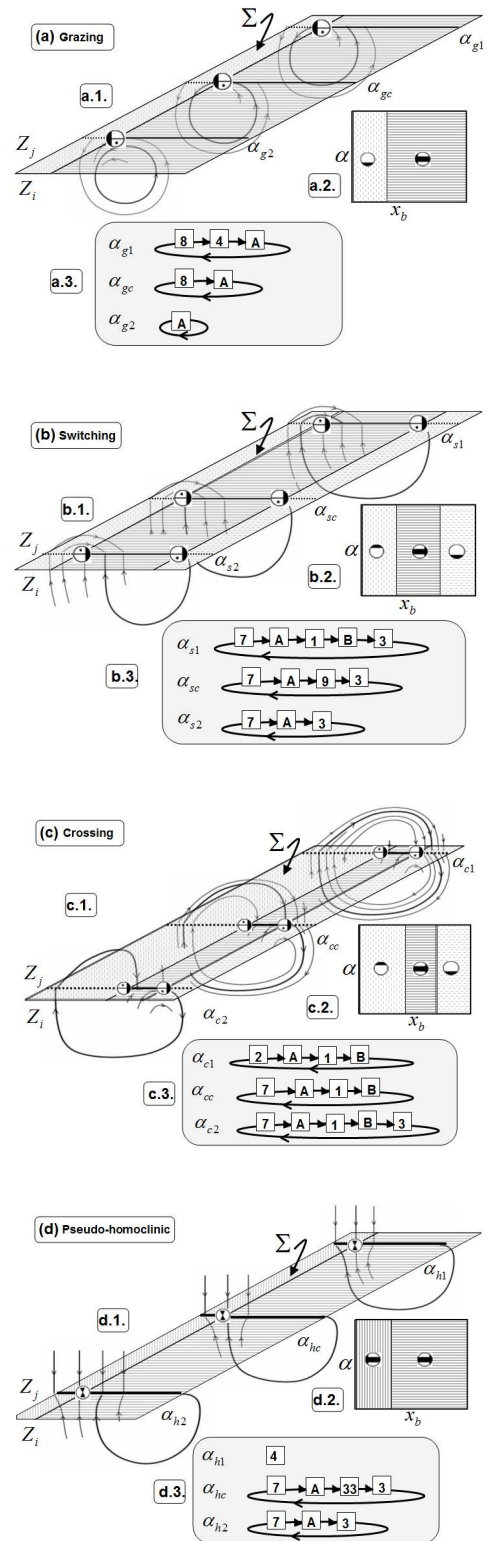


Figure 7: (1). Phase portraits of Global bifurcations. (2). DB bifurcation diagram. (3). Singular point sequences. (a) Grazing bifurcation (b). Switching bifurcation. (c) Crossing bifurcation. (d). Pseudo-homoclinic bifurcation (VII).

In each scenario, a sequence of three points is determined. The central point is a singular sliding point (Ω). The lateral points are crossing (C) points or nonsingular sliding (S) points. Let \mathbf{x}_{b1} , \mathbf{x}_{b2} and \mathbf{x}_{b3} be three consecutive analysis points on DB. We assume that x_{b2} is a singular sliding point and we characterize the neighboring points (\mathbf{x}_{b1} and \mathbf{x}_{b3}).

- **Change of direction of crossing orbits** ($C_{ij} \leftrightarrow C_{ji}$). The lateral points should be C type (C_{ij} or C_{ji}) and the central point should be contained in the set $\Omega_{cc} = \{\Pi_{rr}, \Pi_{ll}, \Pi_{rl}, \Pi_{lr}, \Psi_r^x, \Psi_x^r, \Psi_l^x, \Psi_x^l, Q_{nj}^{ni}, Q_{ni}^{nj}, \phi_x^x\}$.

$$\Lambda_{cc} = \begin{cases} (\mathbf{x}_{b1}, \mathbf{x}_{b2}, \mathbf{x}_{b3}) = (C_{ij}, \Omega_{cc}, C_{ji}) \\ (\mathbf{x}_{b1}, \mathbf{x}_{b2}, \mathbf{x}_{b3}) = (C_{ji}, \Omega_{cc}, C_{ij}) \end{cases} \quad (27)$$

In equation (27) is presented the generic sequences while some examples are shown in equation (28). The numerical codes of the central point can be {23, 24, 25, 26, 27, 28, 29, 30, 33, 36, 37, 41}.

$$\left\{ \begin{array}{cc} (1, 23, 2) & (2, 24, 1) \\ (1, 26, 2) & (1, 36, 2) \\ (2, 33, 1) & (2, 23, 1) \\ (1, 41, 2) & (2, 25, 1) \end{array} \right\} \quad (28)$$

- **Change of crossing boundary to stable sliding boundary, and vice versa** ($C_{ij} \leftrightarrow S_s^l, C_{ij} \leftrightarrow S_s^r, C_{ji} \leftrightarrow S_s^l, C_{ji} \leftrightarrow S_s^r$). The lateral points should be C type or S_s and the central point should be Ω_{css} type where $\Omega_{css} = \{T^s, V^s, \Phi^s\}$.

$$\Lambda_{css} = \begin{cases} (\mathbf{x}_{b1}, \mathbf{x}_{b2}, \mathbf{x}_{b3}) = (C, \Omega_{css}, S_s) \\ (\mathbf{x}_{b1}, \mathbf{x}_{b2}, \mathbf{x}_{b3}) = (S_s, \Omega_{css}, C) \end{cases} \quad (29)$$

The numerical codes of the central point can be {7, 8, 9, 10, 15, 16, 17, 18, 37, 38, 41}. The generic sequences are given in equation (29) and some examples are presented in equation (30).

$$\left\{ \begin{array}{cc} (1, 8, 4) & (3, 7, 2) \\ (4, 16, 1) & (2, 15, 3) \\ (2, 38, 4) & (3, 38, 2) \\ (3, 37, 1) & (2, 15, 3) \end{array} \right\} \quad (30)$$

- **Change of crossing boundary to unstable sliding boundary, and vice versa** ($C_{ij} \leftrightarrow S_u^l$,

$C_{ij} \leftrightarrow S_u^r, C_{ji} \leftrightarrow S_u^l, C_{ji} \leftrightarrow S_u^r$). The lateral points should be C type or S_u and the central point should be Ω_{cus} type where $\Omega_{cus} = \{T^u, V^u, \Phi^u\}$.

$$\Lambda_{cus} = \begin{cases} (\mathbf{x}_{b1}, \mathbf{x}_{b2}, \mathbf{x}_{b3}) = (C, \Omega_{cus}, S_u) \\ (\mathbf{x}_{b1}, \mathbf{x}_{b2}, \mathbf{x}_{b3}) = (S_u, \Omega_{cus}, C) \end{cases} \quad (31)$$

The numerical codes of the central point can be {11, 12, 13, 14, 19, 20, 21, 22, 37, 39, 40}. The generic sequences are given in equation (31) and some examples are presented in equation (32).

$$\left\{ \begin{array}{cc} (1, 12, 6) & (5, 13, 1) \\ (6, 21, 1) & (2, 14, 6) \\ (5, 39, 1) & (2, 19, 6) \\ (2, 40, 6) & (1, 39, 6) \end{array} \right\} \quad (32)$$

- **Change of direction of stable sliding boundary.** ($S_s^l \leftrightarrow S_s^r$). The lateral points should be S_s^l or S_s^r types and the central point should be Q^s type where $Q^s = \{Q_{jr}^{jl}, Q_{jl}^{jr}, Q_{nj}^{ni}\}$.

$$\Lambda_{slr} = \begin{cases} (\mathbf{x}_{b1}, \mathbf{x}_{b2}, \mathbf{x}_{b3}) = (S_s^l, Q^s, S_s^r) \\ (\mathbf{x}_{b1}, \mathbf{x}_{b2}, \mathbf{x}_{b3}) = (S_s^r, Q^s, S_s^l) \end{cases} \quad (33)$$

Six different sequences given by (33) can be defined. These possibilities are presented in equation (34). The numerical codes of the central point can be {31, 32, 33}.

$$\left\{ \begin{array}{cc} (3, 31, 4) & (4, 32, 3) \\ (4, 31, 3) & (3, 33, 4) \\ (3, 32, 4) & (4, 33, 3) \end{array} \right\} \quad (34)$$

- **Change of direction of unstable sliding boundary.** ($S_u^l \leftrightarrow S_u^r$). The lateral points should be S_u^l or S_u^r types and the central point should be Q^u type where $Q^u = \{Q_{ir}^{il}, Q_{il}^{ir}, Q_{ni}^{nj}\}$.

$$\Lambda_{ulr} = \begin{cases} (\mathbf{x}_{b1}, \mathbf{x}_{b2}, \mathbf{x}_{b3}) = (S_u^l, Q^u, S_u^r) \\ (\mathbf{x}_{b1}, \mathbf{x}_{b2}, \mathbf{x}_{b3}) = (S_u^r, Q^u, S_u^l) \end{cases} \quad (35)$$

Six different sequences given by (35) can be defined. These possibilities are presented in equation (36). The numerical codes of the central point can be {34, 35, 36}.

$$\left\{ \begin{array}{cc} (5, 34, 6) & (6, 35, 5) \\ (6, 34, 5) & (5, 36, 6) \\ (5, 35, 6) & (6, 36, 5) \end{array} \right\} \quad (36)$$

- **Change of stability in sliding boundary.** ($S_s^l \leftrightarrow S_u^l, S_s^r \leftrightarrow S_u^r$). The lateral points should be S type and the central point should be Ω_{us} type where $\Omega_{us} = \{\Pi, \Psi\}$.

$$\Lambda_{us} = \left\{ \begin{array}{l} (\mathbf{x}_{b1}, \mathbf{x}_{b2}, \mathbf{x}_{b3}) = (S_s, \Omega_{us}, S_u) \\ (\mathbf{x}_{b1}, \mathbf{x}_{b2}, \mathbf{x}_{b3}) = (S_u, \Omega_{us}, S_s) \end{array} \right. \quad (37)$$

The numerical codes of the central point can be $\{23, 24, 25, 26, 27, 28, 29, 30\}$. The generic sequences are given in equation (37) and some examples are presented in equation (38).

$$\left\{ \begin{array}{ll} (5, 23, 3) & (6, 28, 4) \\ (4, 24, 6) & (4, 30, 6) \\ (5, 26, 3) & (3, 29, 5) \end{array} \right\} \quad (38)$$

- **Change of direction in the velocity of stable sliding boundary:** Both lateral points stable sliding point with the same direction, but a measure that can be associated with the velocities on sliding boundary are different.

$$\Lambda_{vs} = \left\{ \begin{array}{l} (\mathbf{x}_{b1}, \mathbf{x}_{b2}, \mathbf{x}_{b3}) = (S_s^l, Q^s, S_s^l) \\ (\mathbf{x}_{b1}, \mathbf{x}_{b2}, \mathbf{x}_{b3}) = (S_s^r, Q^s, S_s^r) \end{array} \right. \quad (39)$$

The following boolean-valued function is TRUE:

$$B(\Delta_{Gt}(\mathbf{x}_{b1}) > 0) \wedge B(\Delta_{Gt}(\mathbf{x}_{b3}) < 0)$$

where,

$$\Delta_{Gt}(\mathbf{x}_{bi}) = |G_t(\mathbf{x}_{bi})| - |G_t(x_{bi} + \delta)|$$

Six different sequences given by (39) can be defined. These possibilities are presented in equation (40). The numerical codes of the central point can be $\{31, 32, 33\}$.

$$\left\{ \begin{array}{ll} (3, 31, 3) & (4, 31, 4) \\ (3, 32, 3) & (4, 32, 4) \\ (3, 33, 3) & (4, 33, 4) \end{array} \right\} \quad (40)$$

In Filippov systems, the periodic solutions or cycles can be divided in *standard* (L_{st}), *sliding* (L_s) or *crossing* (L_c) cycles. We can use the set of points characterized previously to define the characteristic sequences of each cycle.

- **Standard cycles L_{st} :**

In the standard cycles, the flow lies entirely in Z_i or Z_j zone. Two basic cases can be defined.

If the flow lies entirely in Z_i : $\Phi_a(\mathbf{x}, t_0) = \Phi_a(\mathbf{x}, t_0 + t_\sigma)$ where t_σ is the time period of the cycle. The sequence associate to this standard cycle is denoted by $A \downarrow$ and it is presented in figure 5 (a).

If the flow lies entirely in Z_j : $\Phi_b(\mathbf{x}, t_0) = \Phi_b(\mathbf{x}, t_0 + t_\sigma)$. The sequence associate to this standard cycle is denoted by $B \downarrow$ and it is presented in figure 5 (b).

- **Crossing cycles L_c :**

The crossing cycles have crossing or singular sliding points (Type C or Ω) on DB. The flow passes from Z_i to Z_j or from Z_j to Z_i without sliding motion.

An example of crossing cycle is presented in figure 5 (e). The periodic sequence of this example is $(2, A, 1, B) \downarrow$

- **Sliding cycles L_s :**

The sliding cycles have a sliding stable points (S_s^l or S_s^r) on DB. The sliding cycles can have flow in one or more vector fields.

In figure 5 (g), the sliding cycle only includes flow in Z_i . The characteristic sequence is $(7, A, 3) \downarrow$.

In figure 5 (h), the sliding cycle includes flow in Z_i and Z_j . The characteristic sequence is $(7, A, 1, B, 3) \downarrow$.

5 SPT Method in Local Bifurcation Analysis

All bifurcations of Filippov systems can be classified as *Local* and *Global* bifurcations [18]. The local bifurcations can be detected analyzing the points on the discontinuity boundary.

Let n_Ω be the number of singular points on DB. Therefore, a sequence of $(2n_\Omega + 1)$ points can be determined: $(\mathbf{x}_{b1}, \mathbf{x}_{b2}, \dots, \mathbf{x}_{b(2n_\Omega+1)})$.

The points: $(\mathbf{x}_{b1}, \mathbf{x}_{b3}, \dots, \mathbf{x}_{b(2n_\Omega+1)})$ are crossing points ($C = \{C_{ij}, C_{ji}\}$) or nonsingular sliding points ($S = \{S_s^r, S_s^l, S_u^r, S_u^l\}$). The other points: $(\mathbf{x}_{b2}, \mathbf{x}_{b4}, \dots, \mathbf{x}_{b(2n_\Omega)})$ are singular points ($\Omega = \{T, V, \Pi, \Psi, Q, \phi\}$).

The existence of singular sliding points on DB determines the existence of the events on DB. The

change of the event type when the parameter vector \mathbf{p} is varied determines the existence of nonsmooth bifurcations. The bifurcation points can be detected of several ways. Changes in the number of the singular points on DB or the events on DB when \mathbf{p} is varied imply the existence of bifurcation points. Also, the intersection of two or more singular point curves implies a bifurcation point in the intersection point.

| Bif | \mathbf{F}_i | \mathbf{F}_j | $H(\mathbf{x})$ |
|-----|--|---|-----------------|
| BN1 | $\begin{pmatrix} -3x_1 - x_2 \\ -x_1 - 3x_2 \end{pmatrix}$ | $\begin{pmatrix} 0 \\ -1 \end{pmatrix}$ | $x_2 + \alpha$ |
| BF5 | $\begin{pmatrix} -x_1 - 2x_2 \\ 4x_1 + 2x_2 \end{pmatrix}$ | $\begin{pmatrix} 0 \\ 1 \end{pmatrix}$ | $x_2 + \alpha$ |
| DT1 | $\begin{pmatrix} 1 \\ \alpha + x_1^2 \end{pmatrix}$ | $\begin{pmatrix} 0 \\ -1 \end{pmatrix}$ | x_2 |
| VV2 | $\begin{pmatrix} -1 \\ \alpha + x_1 \end{pmatrix}$ | $\begin{pmatrix} 1 - x_1 \\ x_1 \end{pmatrix}$ | x_2 |
| VII | $\begin{pmatrix} 1 - x_1 \\ \alpha + x_1 \end{pmatrix}$ | $\begin{pmatrix} 1 - x_1 \\ 2x_1 \end{pmatrix}$ | x_2 |
| PSN | $\begin{pmatrix} \alpha + x_1^2 \\ 1 \end{pmatrix}$ | $\begin{pmatrix} 0 \\ -1 \end{pmatrix}$ | x_2 |

Table 1: Configurations $\{\mathbf{F}_i, \mathbf{F}_j, H\}$ of topological normal forms of local bifurcations.

In [18] the codimension-one nonsmooth bifurcations were classified. Next, we present the general consideration to detect the local nonsmooth bifurcations using the SPT method. A *normal chain* $\Lambda_N(\mathbf{x}_b, \mathbf{p}) = \{\Lambda_1(\mathbf{x}_b, \mathbf{p}_1), \Lambda_2(\mathbf{x}_b, \mathbf{p}_2), \Lambda_3(\mathbf{x}_b, \mathbf{p}_3)\}$ can be defined in each case when the parameter vector \mathbf{p} is varied. The central element $\Lambda_2(\mathbf{x}_b, \mathbf{p}_2)$ reproduces the behavior in the critic value of \mathbf{p} , while side elements have the behavior before an after the bifurcation, respectively.

The equilibrium points of the vector fields \mathbf{F}_i or \mathbf{F}_j can collide with the discontinuity boundary. When a hyperbolic equilibrium collides with the DB, the system has a *Boundary-Equilibrium bifurcation*. Depending of the equilibrium type the bifurcation is denoted as Boundary-Focus (BF), Boundary-Node (BN) or Boundary-Saddle (BS).

$$BF1 = \begin{cases} \Lambda_1(\mathbf{x}_b, \mathbf{p}_1) = (C_{ji}, T_j^{sl}, S_s^l) \\ \Lambda_2(\mathbf{x}_b, \mathbf{p}_2) = (C_{ji}, \phi_x^{ni}, S_s^l) \\ \Lambda_3(\mathbf{x}_b, \mathbf{p}_3) = (C_{ji}, T_i^{sr}, S_s^r, Q_{nj}^{ni}, S_s^l) \end{cases} \quad (41)$$

The BF, BN and BS bifurcations are characterized by the intersection between a tangent curve T and a pseudo-equilibrium curve Q when the parameter is varied. In the bifurcation point the system has

a singular point type V or type ϕ .

$$BN2 = \begin{cases} \Lambda_1(\mathbf{x}_b, \mathbf{p}_1) = (C_{ij}, T_i^{ur}, S_u^r, Q_{ni}^{nj}, S_u^l) \\ \Lambda_2(\mathbf{x}_b, \mathbf{p}_2) = (C_{ij}, \phi_x^{nj}, S_u^l) \\ \Lambda_3(\mathbf{x}_b, \mathbf{p}_3) = (C_{ij}, T_i^{ul}, S_u^l) \end{cases} \quad (42)$$

Examples of BF, BN and BS bifurcations are presented in the equations (41), (42) and (43), respectively.

$$BS3 = \begin{cases} \Lambda_1(x_b, p_1) = (S_s^l, T_i^{sl}, C_{ji}) \\ \Lambda_2(x_b, p_2) = (S_s^l, \phi_x^{ni}, C_{ji}) \\ \Lambda_3(x_b, p_3) = (S_s^l, Q_{nj}^{ni}, S_s^r, T_i^{sr}, C_{ij}) \end{cases} \quad (43)$$

Figure 6 shows the bifurcation diagrams and characteristic sequences of BN1 and BF5 bifurcations. The topological normal forms are given in 1.

The collisions of two tangent points when a parameter is varied are local codim 1 bifurcations. In [18] these bifurcations are classified depending the characteristics of the tangent points in the following classes: *Double tangency* (DT), *Visible-Visible* tangencies (VV), *Visible-Invisible* tangencies (VI) and *Invisible-Invisible* tangencies (II).

$$VV1 = \begin{cases} \Lambda_1(\mathbf{x}_b, \mathbf{p}_1) = (S_s^r, T_i^{sr}, C_{ji}, T_j^{ur}, S_u^r) \\ \Lambda_2(\mathbf{x}_b, \mathbf{p}_2) = (S_s^r, \Pi_{rr}, S_u^r) \\ \Lambda_3(\mathbf{x}_b, \mathbf{p}_3) = (S_s^r, T_j^{sr}, C_{ij}, T_i^{ur}, S_u^r) \end{cases} \quad (44)$$

To detect DT, VV, VI and II bifurcations we can track the tangent curves T and determine the bifurcation point when a point type Π or Ψ is detected. The *normal chains* for VV1 and VI2 bifurcations are presented in the equations (44) and (45), respectively.

$$VI2 = \begin{cases} \Lambda_1(\mathbf{x}_b, \mathbf{p}_1) = (S_s^l, T_i^{sl}, C_{ji}, T_j^{ur}, S_u^r, Q_{il}^{jr}, S_u^l) \\ \Lambda_2(\mathbf{x}_b, \mathbf{p}_2) = (S_s^l, \Pi_{ll}, S_u^l) \\ \Lambda_3(\mathbf{x}_b, \mathbf{p}_3) = (S_s^l, Q_{jl}^{ir}, S_s^r, T_j^{sr}, C_{ij}, T_i^{ul}, S_u^l) \end{cases} \quad (45)$$

Figure 6 shows the bifurcation diagrams and characteristic sequences of DT1, VV2 and VII bifurcations. The topological normal forms are given in 1.

6 SPT Method in Global Bifurcation Analysis

To analyze global bifurcations which involve sliding on the discontinuity boundary the integration is un-

avoidable, however using the SPT method explained previously, we can determine the initial condition of the integration to reduce the compute time.

Grazing, crossing and switching bifurcations can be detected easily using SPT method. In the critic values the cycles are denoted by L_g , L_{cr} and L_{sw} , respectively.

A *normal sequences* $\Phi_N(\mathbf{x}_b, \mathbf{p}, t) = \{\Phi^1(\mathbf{x}, \mathbf{p}_1, t), \Phi^2(\mathbf{x}, \mathbf{p}_2, t), \Phi^3(\mathbf{x}, \mathbf{p}_3, t)\}$ can be defined in each case when the parameter vector \mathbf{p} is varied. The central element $\Phi^2(\mathbf{x}, \mathbf{p}_2, t)$ reproduces the behavior in the critic value of \mathbf{p} , while side elements have the behavior before an after the bifurcation, respectively.

The Filippov system has a grazing bifurcation point when a standard cycle collides with the DB in a tangent point T . The tangent point should be contained in the subset $T^s = \{T_i^{sr}; T_i^{sl}; T_j^{sr}; T_j^{sl}\}$.

$$G_g = \begin{cases} \Phi^1(\mathbf{x}, \mathbf{p}_1, t) = L_s \\ \Phi^2(\mathbf{x}, \mathbf{p}_2, t) = L_g \\ \Phi^3(\mathbf{x}, \mathbf{p}_3, t) = L_{st} \end{cases} \quad (46)$$

The *normal sequence* of grazing bifurcation is presented in the equation (46). The initial condition $\Phi(t_0)$ of the orbit is the tangent point T . If the tangent vector field in T is \mathbf{F}_i (points: T_i^{sr} or T_i^{sl}) then we integrate the equation $\dot{\mathbf{x}} = \mathbf{F}_i(\mathbf{x}, \mathbf{p})$. Otherwise, if the tangent vector field in T is \mathbf{F}_j (points: T_j^{sr} ; T_j^{sl}) then we integrate the equation $\dot{\mathbf{x}} = \mathbf{F}_j(\mathbf{x}, \mathbf{p})$. In the equation (47), the conditions of the flow in grazing bifurcation are summarized.

$$\begin{cases} \Phi^1(t_0) = T; \Phi^1(t_1) = S_s; \Phi^1(\mathbf{x}_b, t) \notin C \\ \Phi^2(t_0) = T; \Phi^2(t_0 + kt_\sigma) = T; \Phi^2(\mathbf{x}_b, t) \notin \{S, C\} \\ \Phi^3(t_0) = T; \Phi^3(\mathbf{x}, t) \notin \Sigma \end{cases} \quad (47)$$

The crossing bifurcation point happens when a crossing cycle returns to tangent point without sliding points on DB. Both field vectors F_i and F_j should be integrated to verify the crossing bifurcation. The *normal sequence* of crossing bifurcation is presented in the equation (48).

$$G_{cr} = \begin{cases} \Phi^1(\mathbf{x}, \mathbf{p}_1, t) = L_s \\ \Phi^2(\mathbf{x}, \mathbf{p}_2, t) = L_{cr} \\ \Phi^3(\mathbf{x}, \mathbf{p}_3, t) = L_c \end{cases} \quad (48)$$

The initial condition $\Phi(t_0)$ of the orbit is the tangent point T . If the tangent vector field in T is \mathbf{F}_i (points: T_i^{sr} or T_i^{sl}) then we integrate the equation $\dot{\mathbf{x}} = \mathbf{F}_i(\mathbf{x}, \mathbf{p})$. In a time t_σ the crossing cycle L_{cr} returns to the tangent point T without sliding points on

DB. In the equation (49), the conditions of the flow in grazing bifurcation are summarized.

$$\begin{cases} \Phi^1(t_0) = T; \Phi^1(t_1) = S_s; \Phi^1(\mathbf{x}_b, t) \notin C \\ \Phi^2(t_0) = T; \Phi^2(t_1) = C; \Phi^2(t_2) = T \\ \Phi^2(\mathbf{x}_b, t) \notin S \\ \Phi^3(t_0) = T; \Phi^3(t_1) = C; \Phi^3(t_2) = S_s \end{cases} \quad (49)$$

In the switching bifurcation point the solution travels an entire stable sliding segment and returns to a tangent point defined as initial condition T_1 . Two tangent points T_1 and T_2 are necessary in the switching bifurcation. The initial condition T_1 is defined depending of the sliding segment direction.

$$G_{sw} = \begin{cases} \Phi^1(\mathbf{x}, \mathbf{p}_1, t) = L_s \\ \Phi^2(\mathbf{x}, \mathbf{p}_2, t) = L_{sw} \\ \Phi^3(\mathbf{x}, \mathbf{p}_3, t) = L_s \end{cases} \quad (50)$$

The *normal sequence* of switching bifurcation is presented in the equation (50). The switching cycle L_{sw} arrives of T_1 to T_2 in a time t_1 , after the solution slides and returns to T_1 in a time t_2 without crossing points on DB. In the equation (51), the conditions of the flow in switching bifurcation are summarized.

$$\begin{cases} \Phi^1(t_0) = T_1; \Phi^1(t_1) = S_s; \Phi^1(\mathbf{x}_b, t) \notin C \\ \Phi^2(t_0) = T_1; \Phi^2(t_1) = T_2; \Phi^2(t_2) = T_1 \\ \Phi^2(\mathbf{x}_b, t) \notin C \\ \Phi^3(t_0) = T_1; \Phi^3(t_1) = C; \Phi^3(t_2) = S_s \end{cases} \quad (51)$$

Figure 7 shows the bifurcation diagrams and characteristic sequences of grazing, crossing and switching bifurcations.

7 Illustrative Example

In this section, we study a mechanical system using the SPT method. The system selected is a friction oscillator composed by a cam-follower system and a mass slider.

The chosen cam is a cylindrical or drum cam. This cam can have symmetrical cam profile or asymmetrical cam profile. The mass slider m is mounted on a follower element which runs forward with a speed v .

A schematic drawing of the mechanical system is shown in figure 8(a). According to the model described in figure 8(a) we can plot the free body diagram as shown in figure 8(b) where $F_i = m\ddot{x}$ represents the inertial force of the mass slider and F_f represents the friction force. Therefore,

$$m\ddot{x} = F_f$$

Let v_r be the relative velocity defined as the difference between the follower velocity and the mass slider velocity: $v_r = v - \dot{x}$. Depending on the direction of static friction force, the mass slider can present sliding or not.

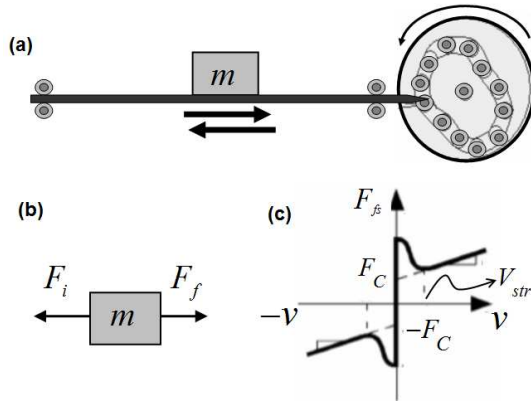


Figure 8: Cam-follower with mass slider. (a). Schematic drawing of the mechanical system. (b). Free body diagram. (c). Friction force curve.

The friction force is expressed as equation (52) where the friction force depends on the follower acceleration. When the follower velocity no changes, the friction force is zero.

$$F_{fs} = (m\dot{v})(\text{sign}(\dot{v}))(\text{sign}(v)) \quad (52)$$

During sliding, the friction model is given by equation (53) where σ_2 is the viscous friction coefficient, F_C is the Coulomb friction, v_{str} is the stiction velocity and δ is a shape factor. The friction force curve is shown in figure 8(c).

$$F_{fk} = k_0 + \left[F_C + k_1(\exp(-|k_v|^\delta)) \right] [\text{sign}(v_r)] \quad (53)$$

with,

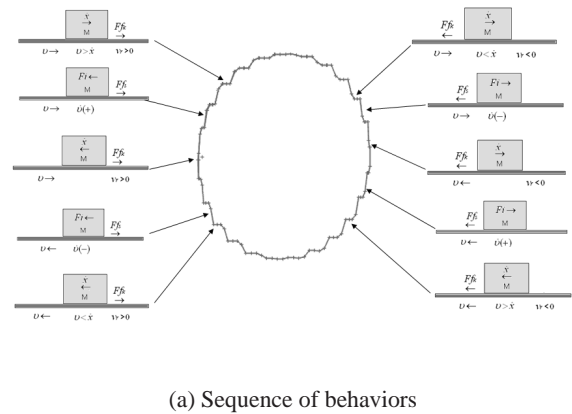
$$\begin{aligned} k_v &= \left(\frac{v_r}{v_r - v_{str}} \right) \\ k_0 &= \sigma_2 v_r \\ k_1 &= (F_{fs} - F_C) \end{aligned}$$

Assuming that x_1 is associated to mass slider position and x_2 is associated to mass slider velocity, the dynamic equation can be expressed as:

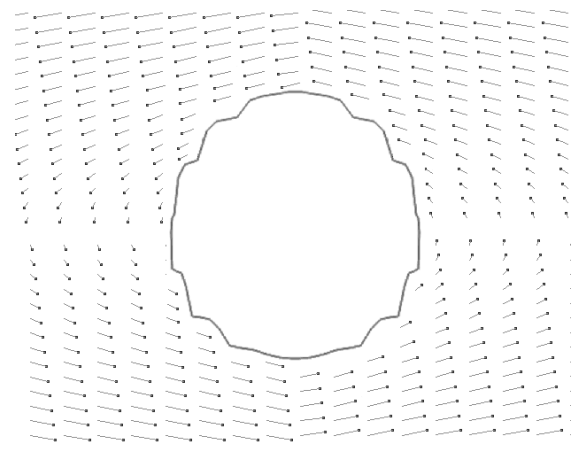
$$\begin{bmatrix} \dot{x}_1 \\ \dot{x}_2 \end{bmatrix} = \begin{bmatrix} x_2 \\ -\frac{F_{fk}}{m}(x_2) \end{bmatrix} \quad (54)$$

The simulation parameters are: Time period (T) is 1 second, Coulomb friction force is 1N, maximum

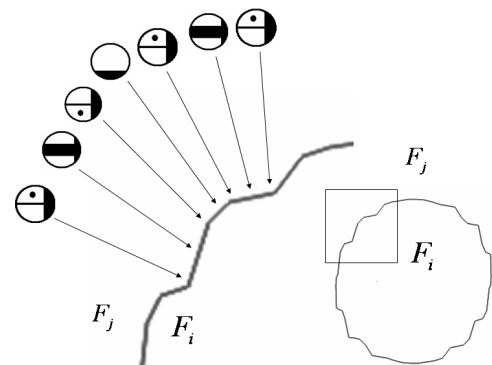
friction force is 1.5N, shape factor δ is 0.79, stiction velocity is 1.5m/s, maximum high cam is 0.05m and dynamic friction coefficient is 0.2.



(a) Sequence of behaviors



(b) Vector fields



(c) Analysis with SPT method

Figure 9: Nonsmooth local dynamics of cam-follower with mass slider. ($\sigma = \pi$, $\omega = 600rpm$)

Using the symmetrical cam profile, the system

is simulated and the phase portrait is created. With $\omega = 600rpm$ the mass presents multi-sliding behaviors. The mass slider behavior is presented in figure 9. The multi-sliding response can be characterized with the type of points on DB.

The multi-sliding orbit is divided into periodic sequences of points: $\{\dots, \Omega_T, S_s, \Omega_T, C, \Omega_T, S_s, \Omega_T \dots\}$. For example, the SPT method detects the sequence: $(\dots, 9, 3, 7, 2, 7, 3, 7, \dots)$ in the piece of flow presented in figure 9(c).

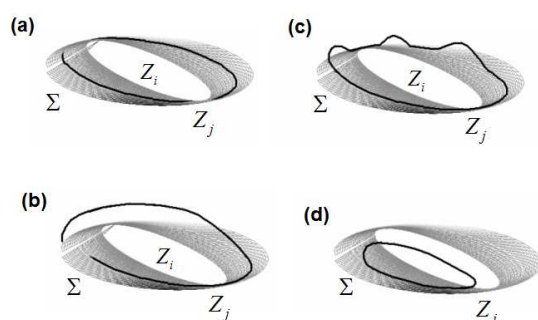


Figure 10: Nonsmooth global dynamics of cam-follower with mass slider.

Global dynamics on cam-follower with slider mass can be studied with SPT method too. For $\omega \approx 60rpm$ the system has standard cycles. Figure 10(a) shows a cycle L_{st} with the sequence: B_i .

For $\omega \approx 120rpm$ the system has multi-sliding cycles. Figure 10(c) shows a cycle L_{ms} with the sequence: $(\Omega_T, B, S_s, \Omega_T, B, S_s, \Omega_T, B)$.

For $\omega > 4000rpm$ the system has sliding cycles. Figure 10(b) and (d) shows a cycle L_s with the sequences: (Ω_T, B, S_s) and (Ω_T, A, S_s) .

8 Conclusion

We have presented the fundamental set of rules behind of the *LabView* toolbox for bifurcation analysis of Filippov systems denominated SPTCont 1.0. We have shown the characteristic point sequences that SPTCont 1.0 detects to guarantee the existence of local and global nonsmooth bifurcations in planar Filippov systems ($n = 2$). Dynamics on DB and cycles have been defined in function of the set of points. The full catalog of codim 1 local and global bifurcations have been used to define the characteristic point sequence when the bifurcation parameter is varied.

References:

- [1] B. Brogliato. *Nonsmooth Mechanics Models, Dynamics and Control*. Springer Verlag, New York, 1999.
- [2] C. J. Budd M. di Bernardo and A. R Champneys. Grazing and border–collision in piecewise smooth systems: a unified analytical framework. *Phys. Rev. Lett*, 86:2553,2556, 2001.
- [3] R. Alzate M. di Bernardo S. Santini, U. Montanaro. Experimental and numerical verification of bifurcations and chaos in cam–follower impacting systems. *to appear in Nonlinear Dynamics (DOI 10.1007/s11071-006-9188-8)*, 2007.
- [4] P. Kowalczyk and M. di Bernardo. Two–parameter degenerate sliding bifurcations in filippov systems. *Physica D–Nonlinear Phenomena*, 204(3-4):204229, May 2005.
- [5] B. Brogliato. *Impacts in Mechanical Systems Analysis and Modelling*. Springer Verlag, New York. Lecture Notes in Physics, Volume 551., 2000.
- [6] F. Dercole Yu. A. Kuznetsov. Slidecont: An auto97 driver for bifurcation analysis of filippov systems. *ACM Trans. Math. Softw*, 31, 95–119, 2005.
- [7] N. Zanzouri A. Zaidi and M. Tagina. Graphical approaches for modelling and diagnosis of hybrid dynamic systems. *WSEAS TRANSACTIONS on SYSTEMS, Issue 10, Volume 5, October 2006*.
- [8] L. Glielmo M. di Bernardo, F. Garofalo and F. Vasca. Switchings, bifurcations and chaos in dc/dc converters. *IEEE Transactions on Circuits and Systems, Part I*, 45:133141, 1998.
- [9] S. Khanmohamadi A. Ghanbari. A new test rig for frictional torque measurement in ball bearings. *WSEAS TRANSACTIONS on SYSTEMS, Issue 9, Volume 5, September 2006*.
- [10] P. Mosterman and G. Biswas. A theory of discontinuities in physycal system models. *El Sevier*, 325B, 1998.
- [11] Sven Hedlund. *Computational Methods for Hybrid Systems*. PhD thesis, Lund Institute of Technology, 1999.
- [12] P.T. Piironen Yu. A. Kuznetsov. An event–driven method to simulate filippov

systems with accurate computing of sliding motions. *Technical report, University of Bristol*, 2005.

- [13] I. Arango and J. A. Taborda. Sptcont 1.0: A lab-view toolbox for bifurcation analysis of filippov systems. *Proceedings of the 12th WSEAS International Conference on Systems, Heraklion, Greece*, 2008, pp. 587–595.
- [14] Iván Arango. *User Guide to Gaondysy*. EAFIT University, 2007.
- [15] I. Arango J. A. Taborda. Integration-free analysis of nonsmooth local dynamics in planar filippov systems. *International Journal of Bifurcation and Chaos*, to appear, 2008.
- [16] I. Arango and J. A. Taborda. Characterizing points on discontinuity boundary of filippov systems. *Proceedings of IASTED International Conference on Modelling, Identification and Control (MIC 2008)*, 2008, Innsbruck, Austria.
- [17] I. Arango and J. A. Taborda. Analyzing sliding bifurcations on discontinuity boundary of filippov systems. *Proceedings of the American Conference on Applied Mathematics (MATH 08)*, Cambridge USA, 2008, pp. 165–170.
- [18] Yu. A. Kuznetsov S. Rinaldi, A. Gragnani. One-parameter bifurcations in planar filippov systems. *International Journal of Bifurcations and Chaos*, 13(8):21572188, 2003.
- [19] R. I. Leine. *Bifurcations in Discontinuous Mechanical Systems of Filippov – Type*. PhD thesis, Technische Universiteit Eindhoven, 2000.
- [20] U. Galvanetto. Some discontinuous bifurcations in a two-block stick-slip system. *Journal of Sound and vibration*, 248(4), 653–669, 2001.
- [21] Leine R.I. H. Nijmeijer. *Dynamics and Bifurcations in Non – Smooth Mechanical Systems*. Springer Verlag, 2004.
- [22] Albert C.J. Luo. A theory for non-smooth dynamic systems on the connectable domains. *Communications in Nonlinear Science and Numerical Simulation*, 10 1–55, 2005.
- [23] A.R. Champneys S.J. Hogan M. Homer Yu.A. Kuznetsov A. Nordmark P. Kowalczyk, M. di Bernardo and P.T. Piiroinen. Two-parameter nonsmooth bifurcations of limit cycles: classification and open problems. *International Journal of Bifurcations and Chaos*, 2006.
- [24] J. A. Ferreira. A review of mathematical models of non-linear mechanical systems that involve friction. *WSEAS TRANSACTIONS on SYSTEMS, Issue 12, Volume 6*, December 2007.
- [25] A. F. Filippov. *Differential equations with discontinuous righthand sides*. Kluwer Academic Publishers, Dordrecht, 1988.